Measurement and Stochastic Computational Modeling of the Elastic Properties of Parallel Strand Lumber

Sanjay R. Arwade, A.M.ASCE[1]; Peggi L. Clouston, A.M.ASCE[2]; and Russell Winans[3]

Abstract: This paper describes a model for the spatial variation of the elastic modulus of parallel strand lumber (PSL) that is based on bending experiments and also describes a validated stochastic computational model that incorporates orthotropic elasticity and uncertainty in strand geometry and material properties. The PSL exhibits significant variability both within members and between members, but this variability is less than that of equivalent sawn-wood members, and decreases with increasing member size. The correlation length of the elastic modulus is found to be several meters and is independent of the cross-sectional size. The variance of PSL elastic modulus is found to scale inversely with the number of strands in the cross section. The validated computational model is flexible enough to allow preliminary exploration of the properties of new mixes of species and strand sizes in PSL material design.

DOI: 10.1061/(ASCE)EM.1943-7889.0000020

CE Database subject headings: Mechanics; Wood; Elasticity; Probability; Random processes; Computation; Laminated wood; Measurement; Stochastic models.

Introduction

Parallel strand lumber (PSL) (Fig. 1) is an engineered wood product that is used frequently in residential construction and increasingly in commercial and industrial applications. PSL is composed of long, thin, narrow strands of wood aligned with the longitudinal axis of the member, which are bonded together under high pressure. It is considered to be an economically and ecologically advantageous material because it uses wood fiber from plywood panel production that would otherwise be waste material. The heterogeneous random composite mesostructure makes the material properties of PSL vary spatially in ways that differ substantially from that of solid lumber.

The goals of this study are to measure the variation of elastic modulus along the length of PSL beams, to develop a probabilistic model for the PSL mesostructure and an accompanying computational model for the elastic mechanics of PSL, and to develop a probabilistic characterization of the spatially varying elastic modulus of PSL members.

This work will advance fundamental understanding of the elastic behavior of PSL, and the computational model developed has predictive capability that should prove useful in developing new material designs for structural composite lumber. Furthermore, the analysis, characterization, and modeling of variation of elastic properties is an important first step toward a comprehensive model for PSL strength properties. The development of such a comprehensive model is important to increasingly rational, probabilistic, design of composite wood structures, and is currently being undertaken by the writers. Finally, this testing and modeling also address the variation of elastic properties between nominally identical members. Characterization of this variation of elastic properties is important to reliability based design for serviceability, whereas strength variation would be important to design for safety.

No previous studies have addressed spatial variability of material properties of PSL; however, work has been done on solid wood (Forest Products Laboratory 1999) and dimensional lumber (Lam and Varoglu 1991a,b; Lam et al. 1994). The *Wood Handbook* gives typical coefficients of variation of elastic constants of solid lumber to be 20%. The latter studies proposed stochastic process models with correlation lengths on the order of 10–100 cm determined from experiments for both strength and stiffness properties.

Though these models provide a starting point for the modeling described here, the present model goes further to account for both variation within a member and between members. Another achievement of this work is to quantitatively describe how the use of bending tests to measure elastic modulus distorts estimates of spatial statistics of the elastic modulus process. This distortion is caused by volume averaging of the material properties that occurs when an effective modulus is estimated from a three point bending test. Such tests can correctly measure the average modulus, but not the properties of the spatial variation of the modulus.

Some preliminary work has shown connections between mesostructure properties and mechanical properties of PSL (Bejo and Lang 2004). The mesostructural model described in this study extends the two dimensional model of Bejo and Lang's work to a three dimensional model.

The treatment of the mechanics of PSL described here builds upon previous work that used nonlinear finite element analysis of PSL to derive effective cross-sectional properties (Clouston and Lam 2001,2002; Clouston 2006). The key advance here is the

[1]Assistant Professor, Dept. of Civil and Environmental Engineering, Univ. of Massachusetts, 223 Marston Hall, Amherst, MA 01003 (corresponding author). E-mail: arwade@ecs.umass.edu

[2]Associate Professor, Dept. of Natural Resources Conservation, Univ. of Massachusetts, Amherst, MA 01003. E-mail: clouston@nrc.umass.edu

[3]Graduate Student, Dept. of Civil and Environmental Engineering, Univ. of Massachusetts, Amherst, MA 01003. E-mail: winans@engin.umass.edu

Note. This manuscript was submitted on April 30, 2008; approved on January 12, 2009; published online on March 6, 2009. Discussion period open until February 1, 2010; separate discussions must be submitted for individual papers. This paper is part of the ***Journal of Engineering Mechanics***, Vol. 135, No. 9, September 1, 2009. ©ASCE, ISSN 0733-9399/2009/9-897–905/$25.00.

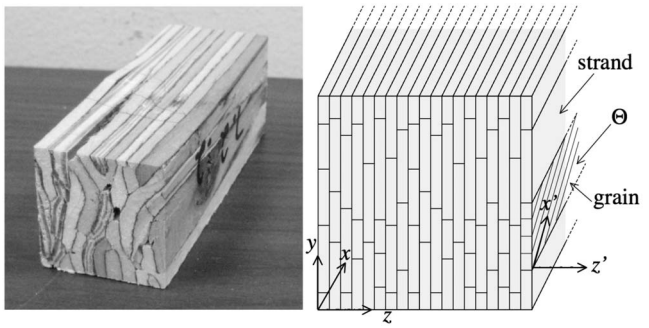

Fig. 1. PSL mesostructure (left) and idealization of PSL mesostructure used in the computational model

addition of the length dimension to the model to allow investigation of spatial variability.

Materials and Methods

The initial material specimen (A1) used in this study is southern yellow pine PSL with length $l_m=4.88$ m and square cross section of width $w=133$ mm. After initial bending tests, this specimen was machined to 9 specimens (B1, B2,…, B9), each with length $l_m=2.44$ m, and square cross-sectional width $w=39$ mm. The strands composing the PSL have roughly rectangular cross section with depth $d_s=5$ mm and width $w_s=13$ mm. The long axis of the strands is roughly aligned with the long axis of the test specimens and the expected number of strands in each specimen cross section is approximately 275 for specimen A1 and 24 for the specimens in Group B. Because the nine B samples are machined from the single A sample, the testing here does not capture variation of properties induced by differences in production runs. There is currently only one manufacturer of PSL, so variation between manufacturers is not an issue.

To measure the elastic modulus of the PSL specimens edgewise bending tests were performed using the setup shown schematically in Fig. 2. The total specimen length is denoted by l_s and the span between test supports is l_t. Lacking access to a Cook-Bolinder type machine capable of making continuous measurement of the stiffness, an approach was adopted in which the test specimen was moved through the test apparatus in discrete increments of length l_p, and load and deflection were measured after each increment of movement.

The test dimensions (Table 1) conform to ASTM D198-05 (ASTM 2005) to ensure bending dominated behavior of the test

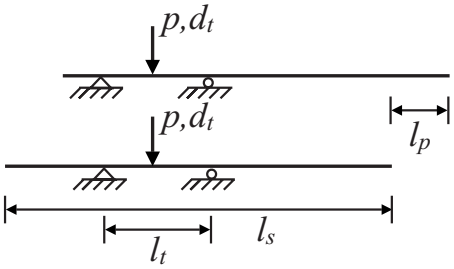

Fig. 2. Bending test setup schematic showing passage of test specimen through loading and support apparatus for sequential modulus of elasticity measurements

Table 1. Bending Test Geometry Parameters

Group	w (mm)	l_m (m)	l_p (mm)	l_t (m)	p (KN)
A	133	4.87	152	2.44	2.2
B	39	2.44	76	0.38	1.3

specimens. All testing was conducted well within the elastic range.

The tests were conducted in the Wood Mechanics lab at the University of Massachusetts, Amherst using a universal material testing system operating in displacement control at a displacement rate of 2.54 mm/min in accordance with the ASTM standard. The applied displacement rate ensures that rate-dependent and viscous effects were negligible during the test (ASTM 2005). During testing, the load was recorded using a 147 KN load cell, and displacement at midspan of the test length was measured by a linear variable displacement transducer placed at the centerline of the test specimen directly under the point of load application.

The tests, designed to measure the bending elastic modulus of the PSL samples, deliver time series $d(t)$ of the midspan displacement and $p(t)$ applied load. With the time acting as a parameter, the load can be expressed as

$$p_i(d,\ E(x),\ w),\ x \in \left[x_i - \frac{l_t}{2},\ x_i + \frac{l_t}{2}\right] \tag{1}$$

where $x_i,\ i=1,\ldots,\ n_t$ is a position along the length of the specimen at which load is applied; $E(x)$=randomly fluctuating effective elastic modulus of the specimen cross section at longitudinal position x; and p_i=load applied at position x_i during testing.

This experiment can capture variation of effective elastic modulus along the length of the member, but not within the cross section. Eq. (1) can be rearranged to the form

$$d_i = \left[\int\int \frac{m(p,u)}{E(u)I}dudu\right]_{u=l_t/2} \quad \text{plus boundary conditions} \tag{2}$$

where u=dummy variable that is equal to 0 at one support and l_t at the other; $m(p,u)$=bending moment resulting from load p; and $I=w^4/12$=moment of inertia, constant over the length of the specimen. The elastic modulus $E(u)$ is the unknown in this equation, yet cannot be solved for uniquely.

Introducing the notation $\bar{E}_i=\langle E(x)\rangle,\ x \in \left(x_i-\frac{l_t}{2}, x_i+\frac{l_t}{2}\right]$ allows the solution of Eq. (2) to give

$$\bar{E}_i = \frac{pl_t^3}{48dI} \tag{3}$$

in which p and d are observed at the same time, but the time argument has been dropped for compactness. The overbar on $\bar{E}_i$ indicates that it is averaged over the volume of material between the supports of the bending test, but it is not an arithmetic average since the value of the modulus at different points in the test span contributes differently to the midspan displacement. The value $\bar{E}_i$ is therefore an average weighted by the mechanics of the bending test and Eq. (2). Any noise in the measurements of d and p is neglected.

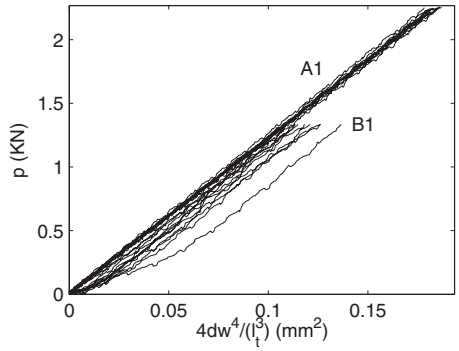

Fig. 3. Load-displacement curves from bending tests normalized to show material stiffness

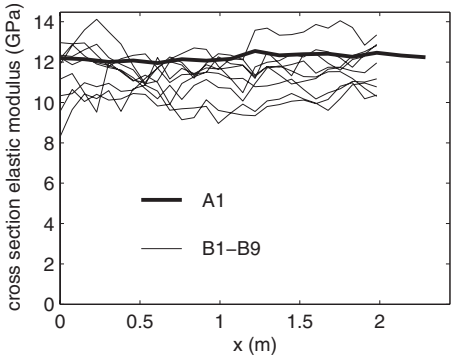

Fig. 4. Experimental observations of cross-sectional elastic modulus random process $\bar{E}(x)$

Experimental Results

The bending tests measure the cross-sectional elastic modulus at 16 points along the length of specimen A1, and at 27 points along the length of each of the Group B specimens, a total of 259 elastic modulus measurements.

Fig. 3 shows the load-displacement response of the test samples with the quantity $48dI/l_t^3$ replacing the displacement d. This substitution allows the effective cross-section elastic modulus $\bar{e}_i$ to be read directly as the slope of the curve $(p,\ 48dI/l_t^3)$. Note that $\bar{e}_i$ is written in lower case to indicate that this is a realization of the observation $\bar{E}_i$ of the underlying random process $\bar{E}(x)$. A small nonlinearity at the beginning of each test reflects seating of the specimen and fixture rather than the actual PSL mechanics. The linear portion of each test curve was selected manually and the effective cross-section elastic modulus was calculated using the parts of the curve between about 0.45 and 1.1 KN for the B specimens and between about 0.45 and 1.8 KN for the A specimen.

The statistics of the tests are shown in Table 2. The main comparison is between the mean and standard deviation of sample A1 and the aggregate statistics for the B samples. The B samples, with smaller cross section and shorter test span length show a moderately lower mean elastic modulus and a dramatically higher standard deviation of the elastic modulus. Specifically, the coefficient of variation of $\bar{E}$ for the A sample is 1.4% and for the B samples is 9.1%.

Table 2. Bending Test Result Statistics

Sample	Mean (GPa)	Standard deviation (GPa)	Skewness	Kurtosis
A1	12.2	0.172	—	—
B1	12.1	0.758	—	—
B2	12.6	0.896	—	—
B3	11.2	0.689	—	—
B4	12.0	0.565	—	—
B5	11.5	0.655	—	—
B6	10.7	0.524	—	—
B7	11.8	0.579	—	—
B8	10.3	0.758	—	—
B9	10.0	0.620	—	—
B ensemble	11.4	1.03	0.038	2.80
B means	—	0.876	—	—
B standard deviations	0.676	—	—	—

The lower mean elastic modulus of the B samples is not readily explained, but the difference is small, approximately 7%, and could be an artifact of the availability of only a single A sample. The difference in coefficient of variation, however, is expected, and can be logically attributed to the smaller cross-sectional area, shorter test span length, and lower test load level. The smaller cross-sectional area of the B samples results in fewer strands being included in the cross section. The smaller cross section and shorter test span decrease the volume of material in which elastic modulus averaging is taking place, and tends to increase the variability of the estimate of $\bar{E}$.

The results of Table 2 show that the total variability of $\bar{e}_i$ is a combination of specimen-to-specimen variation and within-specimen variation. The total standard deviation of all B specimen measurements is 1.03 GPa, and these measurements have skewness close to zero and kurtosis near 3. The total standard deviation corresponds to a coefficient of variation of approximately 9%, which is substantially lower than typical 20% coefficients of variation for solid lumber. The standard deviation of the mean value of $\bar{e}_i$ for each of the nine test specimens, 0.876 GPa, quantifies the specimen-to-specimen variability of the effective elastic modulus. The mean value of the standard deviations of the 27 measurements taken within each sample is 0.676 GPa and quantifies the within-specimen variability of the effective elastic modulus. Based on these test data, 63% of the total variance is attributable to specimen-to-specimen variability, and 37% to within-specimen variability.

Fig. 4 both illustrates the dramatically smaller variability of the A sample and the within-member and across member variation of the B sample elastic moduli. Specifically, the B sample curves have different mean values, indicating the member-to-member variation. Each B sample curve, in turn, shows fluctuations about its own mean, indicating within-member variation. The sample plots also suggest that the elastic modulus process is stationary in its mean, which has not been observed in solid lumber (Lam et al. 1994).

The experimental tests provide realizations of observations $\bar{e}_i=\bar{e}(x_i)$ of the random process $\bar{E}(x)$. This random process is assumed to be stationary based on the experimental results of Fig. 4 and the known manufacturing process of PSL. The assumption of ergodicity of the random process seems reasonable, yet any approximate test of ergodicity would require extremely long samples of many tens or hundreds of meters, which cannot be

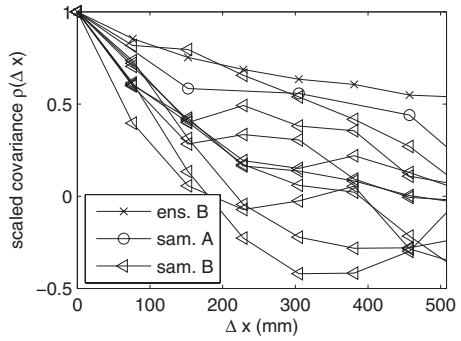

Fig. 5. Scaled covariance functions for A and B samples estimated by sample and ensemble methods for B samples and sample method for the A sample

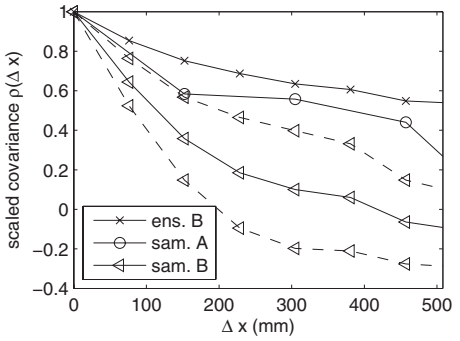

Fig. 6. Summary of scaled covariance functions for A and B samples estimated by sample and ensemble methods for B samples and sample method for the A sample showing for the B samples the mean plus and minus one standard deviation of the sample covariances

obtained or tested. The data shown in Fig. 4 show that using the assumption of ergodicity to estimate statistics of $\bar{E}(x)$ would lead to incorrect conclusions. Specifically, the mean of any one of the B samples is not equal to the ensemble mean of the B samples.

The simplest characterization of the spatial variation of a stationary random process $Y(x)$ is the autocovariance function, which, in its scaled form, is

$$\rho(\Delta x) = \frac{\langle (Y(x) - \langle Y(x) \rangle)(Y(x+\Delta x) - \langle Y(x+\Delta x) \rangle) \rangle}{\sigma_Y^2} \tag{4}$$

where Δx=separation distance and σ_Y=standard deviation of $Y(x)$. Sample and ensemble estimates of the scaled autocovariance will differ substantially if the process is not ergodic, or if samples of insufficient length are used in the sample estimation.

Consider a weakly stationary process $Y(x)$ for which sample observations $y_{ij}=y_i(x_j)$ are available at points x_j, $j=1,\ldots,m_o$ for samples $y_i(x)$, $i=1,\ldots,m_s$. The first subscript indicates the sample number and the second subscript the position at which the observation is made. Assume that the observations are evenly spaced. The sample estimate of the scaled autocovariance for $\tau=k(x_{j+1}-x_j)$ with k an integer is given, for sample $y_i(x)$ by

$$\rho(\Delta x) \approx \frac{1}{m_o - k} \sum_{j=1}^{m_o-k} \left(y_{ij} - \frac{1}{m_o} \sum_{j=1}^{m_o} y_{ij} \right) \left(y_{ij+k} - \frac{1}{m_o} \sum_{j=1}^{m_o} y_{ij} \right) \tag{5}$$

The ensemble estimate of the scaled autocovariance is given by

$$\rho(\Delta x) \approx \frac{1}{m_s(m_o - k)} \sum_{i=1}^{m_s} \sum_{j=1}^{m_o-k} \left(y_{ij} - \sum_{i=1}^{m_s} \sum_{j=1}^{m_o} y_{ij} \right) \left(y_{ij+k} - \sum_{i=1}^{m_s} \sum_{j=1}^{m_o} y_{ij} \right) \tag{6}$$

These expressions show that not only does ensemble estimation tend to be based on a much larger number of observations, but also uses an estimate of the mean of the process that differs qualitatively from that used in sample estimation when the process is nonergodic or the individual samples are short. Ensemble estimates of the scaled covariance function will therefore tend to indicate a much slower decay of the covariance than will an estimate based on a single short sample.

Fig. 5 shows the sample estimates of the scaled covariance for sample A1 and each of the B samples. Also shown is the ensemble estimate of the scaled covariance for the B samples. For increased clarity Fig. 6 shows the A sample estimate, the B ensemble estimate, and the average of all the B sample estimates. While acknowledging that the single A sample available is fundamentally insufficient to provide a valid estimate of the scaled covariance for a PSL member with a 133 mm square cross section, some important interpretations of the spatial variability of elastic properties in PSL members remain possible. Note that in both figures the abscissa is truncated at only 508 mm because at longer separations estimation error becomes dominant.

There is enormous scatter in the sample estimates of $\rho(\Delta x)$ for the B samples, a signature of the shortness of the sample length relative to the correlation length of the process. The ensemble estimate of the B sample scaled covariances shows substantially slower decay than all but one of the sample estimates. This observation is in agreement with the preceding analysis, and with the statistics of Table 2, which show substantial variability in the sample estimates of the mean elastic modulus obtained from the nine B samples. Finally, the sample estimate of the scaled covariance for the A sample shows slower decay than that for all but one of the B samples, but more rapid decay than the ensemble estimate for the B samples.

If the correlation length l_c is defined by

$$l_c = \arg \max_{\Delta x} \{ \rho(\Delta x) : |\rho(\Delta x)| > \exp(-1) \} \tag{7}$$

then Fig. 6 shows that, assuming that sample estimates yield shorter correlation lengths than ensemble estimates, the correlation length of the filtered, elastic modulus process $\bar{E}(x)$ is greater than 508 mm for both the A and B samples.

Computational Model

Mesostructural Geometry

In the mesostructural idealization used here (Fig. 1) a reference coordinate system is established relative to the specimen geometry and the following assumptions are made:

1. All strands are rectangular prisms with long edge aligned with the long edge of the test specimen.
2. Strand cross-sectional dimensions are deterministic.
3. No voids exist in the PSL.
4. Resin properties are not considered in the model.
5. Grain orientation is defined by the single random angle Θ.

The length of the strands is modeled as a random variable

$$L_s = 0.610 + 1.82Z \tag{8}$$

in which Z=β-distributed random variable on the interval [0,1] with parameters β and α. The strands have length distributed in

the interval (0.610 m, 2.43 m) in with an expected value in meters of $\langle L_s \rangle = 0.610 + 1.82(\alpha/\alpha+\beta)$, which is consistent with known manufacturing processes. The strand length is modeled as a random variable because one of the goals of this research is to investigate variation of PSL properties along the member length, and a major source of this variation is the set of discontinuities introduced into the mesostructure by strand ends.

Strand Mechanics

Each strand is assumed to be orthotropic elastic with one of the principal material axes aligned with the reference z-coordinate, and the orientation of the other two, orthogonal principal material axes is determined by the grain angle Θ. The assumptions made about the strand geometry and orientation of the strands relative to the reference coordinate system allow use of the 2D plane stress assumption for the response of each strand. Under plane stress assumptions the constitutive matrix C of each strand is defined by two elastic moduli $E_{x'}$, and $E_{y'}$, a Poisson's ratio $\nu_{x'y'}$, and a shear modulus $G_{x'y'}$. Here the x' axis is defined relative to the reference x axis by the grain orientation angle Θ. The constants are modeled as independent Gaussian random variables truncated at zero to avoid negative values. The constitutive matrix C is assumed to be constant within a given strand.

Cross-Sectional Mechanics

A simple rule of mixtures model (Jones 1975) is used to approximate the cross-sectional elastic modulus at position x by

$$E(x) = \frac{1}{n_s} \sum_{i=1}^{n_s} E_x[C(\Theta_i)] \tag{9}$$

where $E_x(C(\Theta_i))$=effective material stiffness in the global x-direction of strand i with grain orientation Θ_i and n_s=number of strands in the cross section. $C(\theta)$ is the stiffness matrix in the strand coordinate system, which is transformed to the principal material coordinate system to obtain E_x and then averaged to produce the effective elastic modulus process. Although the individual strands are orthotropic, anisotropy of the PSL member is not addressed since only the longitudinal modulus E_x is considered. Transverse material stiffnesses are not considered, but would differ from the longitudinal modulus due to strand orthotropy. Note that there are two sources of uncertainty in the constitutive matrix C, the random grain angle and uncertainty of the individual elastic constants at a fixed grain angle.

Bending Test Simulations

Eq. (9) can be used to calculate the corresponding realization $e(x)$ of the cross-section elastic modulus process. Specifically, at every position x along the length of the specimen with simulated mesostructure, Eq. (9) is used to average the effective elastic modulus of the constituent strands to obtain $e(x)$. The realization of $e(x)$ is piecewise constant, with discontinuities and a change in effective cross-section modulus at each strand end since properties are assumed constant within a strand. To obtain the corresponding realization of the filtered cross-sectional elastic modulus process requires the solution of

Table 3. Statistics of Strand Elastic Constants

Constant	Mean	Standard deviation
$E_{x'}$	13 GPa	2.60 GPa
$E_{y'}$	0.820 GPa	0.164 GPa
$\nu_{x'y'}$	0.022	0
$G_{x'y'}$	0.882 GPa	0.176 GPa

$$d_i = \left[\int \int \frac{m(p,u)}{e(u)I} dudu \right]_{u=l_i/2} \text{ plus boundary conditions} \tag{10}$$

which is a version of Eq. (2) after substitution of the realization $e(x)$ of $E(x)$. Once d_i is calculated, substitution into Eq. (3) yields a realization $\bar{e}_i$ of $\bar{E}_i$ the filtered cross-sectional elastic modulus. Eq. (10) is solved using a finite difference approach.

Model Validation

The validation exercise of this section compares simulated elastic modulus processes to those obtained from testing. The parameters described in "Bending test simulations" are set to match those of the tests described in "Computational model." The geometric parameters are set as defined in Table 1, and the number of strands in the cross section is fixed at 275 for simulation of the A sample, and 24 for simulation of the B samples. Strand cross-sectional dimensions are fixed at 5 mm × 13 mm, giving a total cross-sectional area for the simulated A samples of 17,800 mm^2, and for the simulated B samples of 1,550 mm^2.

The random parameters used to define the PSL mesostructure are those of the distributions of the strand length, strand elastic constants, and grain angle. Published values for the mean and standard deviation of the elastic constants are used, choice of the parameters of the β distribution for strand length is made based on the known strand manufacturing process, and the grain angle distribution is adopted from a previous, experimental result.

The parameters of the β distribution for the strand length are $\alpha=5$, $\beta=2$ giving a mean strand length of 1.9 m, and a distribution in which most of the probability mass is concentrated near the upper end of the interval [0.610, 2.43] m. The parameters of the Gaussian distributions used as models for the strand elastic constants are given in Table 3 and are taken from the Wood Handbook (Forest Products Laboratory 1999). These represent 20% coefficient of variation on the elastic and shear modulus, and no variation of Poisson's ratio.

The measurement of grain angles is a topic of current investigation and an automated method for measuring grain angle from x-ray imaging has recently been reported (Ekevad 2004). Here, a previously reported empirical probability mass function (pmf) for grain angle is employed (Fig. 7) (Clouston 2006). This empirical pmf (Fig. 7) was compiled from manual measurements of grain angle obtained by serial sectioning of a PSL specimen. For the purposes of the validation study this pmf is assumed to be characteristic of PSL and is assumed to be symmetric about zero. The empirical pmf has most of its mass near $\theta=0$, indicating that strands in PSL are typically well aligned with the geometry of the member. Grain angle $\theta=90°$ is used to represent a strand with a knot defect. Knots are not explicitly considered in the current model, except that assigning $\theta=90°$ significantly softens it due to the characteristics of the strand orthotropic constitutive matrix.

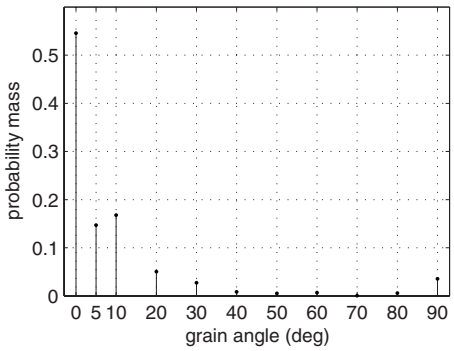

Fig. 7. Probability mass function for grain angle adapted from Clouston (2006)

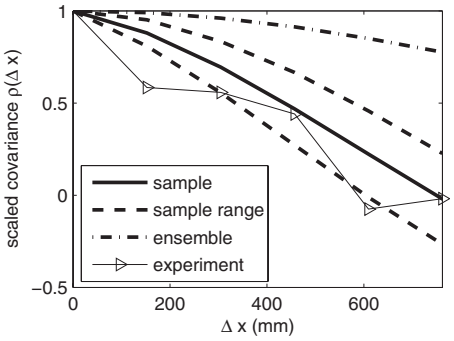

Fig. 8. Experimental and simulated scaled autocovariance functions for A samples estimated by ensemble and sample methods

Validation of the computational model involves generation of 250 independent realizations each of virtual A and B samples, performing virtual bending tests using finite difference calculations on these samples, and estimating statistics of the resulting simulated filtered elastic modulus processes. A convergence study, the details of which are not shown here, demonstrates that with 250 samples the estimation error associated with simulated elastic modulus process statistics is negligible.

The most direct comparison between simulated and experimental results is made between the ensemble statistics for the B samples shown in Tables 4 and 2. The simulations underpredict the mean elastic modulus by 4.3% and underpredict the standard deviation of the elastic modulus by 18%. For a material with the inherent variability and environmental sensitivity of wood, the agreement between the predicted and measured ensemble means is good. That the variability of the elastic modulus is underpredicted by the computational model is expected, and can likely be traced to the omission from the model of voids and within-strand variation of the orthotropic elastic constants. An additional source of variability in the experimental measurements is experimental error which is not quantified here. The skewness and kurtosis values also agree well.

The sample estimates of the simulated B sample test statistics agree with the test data in that the average sample standard deviation is substantially less than the ensemble standard deviation. For the experiments, the mean sample variance is 71% of the ensemble variance, whereas for the simulations the mean sample variance is 29% of the ensemble variance. That the simulations show a mean sample variance lower than the ensemble variance confirms that the individual samples are insufficiently long to capture the spatial variability of PSL. The lower percentage of the ensemble variance that is attributable to within-sample variation in the simulations is likely caused by the omission of the uncertainty and error sources described above.

With only a single A sample available for testing, extensive comparison of the simulation statistics to the experimentally determined statistics is not possible. It suffices to say that the ensemble average mean value of the simulations, 10.8 GPa, and the mean of the simulated sample standard deviations, 0.110 GPa, are not inconsistent with the experimental values of 12.2 GPa and 0.172 GPa. For the simulated A samples, the within-sample variance accounts for 24% of the total variance. This percentage is comparable to that obtained for the simulated B samples, and again reflects that the simulated A samples are insufficiently long to capture the relevant spatial statistics.

Estimates of point statistics of the filtered elastic modulus process obtained from computational simulations agree well with those obtained from experiments, and indicate that the computational model provides a valid prediction of PSL elastic behavior.

Estimates of the scaled autocovariance functions defined in Eqs. (5) and (6) are also obtained from the simulations. Fig. 8 shows the mean plus or minus one standard deviation of the sample scaled autocovariance functions for the 250 simulated A samples along with the ensemble scaled autocovariance function and the single sample scaled autocovariance obtained from experiment. The agreement between the single experimental scaled autocovariance and the simulation results is quite good. At small separation lengths Δx the experimental values are smaller than those obtained from simulation. This is consistent with the observation made from the point statistics that the simulations underestimate elastic modulus uncertainty.

Fig. 9 allows comparison between the simulated and experimental sample and ensemble scaled autocovariance functions for the B samples. As for the A samples, the overall agreement is quite good, with the simulated scaled autocovariances exhibiting slower decay than those obtained experimentally. The difference between the experimental and simulated scaled autocovariances is

Table 4. Bending Test Simulation Statistics

		A samples	*B* samples
Ensemble	Mean (GPa)	10.8	10.8
	Standard deviation (GPa)	0.227	0.848
	Skewness	−0.1	−0.04
	Kurtosis	3.0	3.3
Sample	Mean of standard deviations (GPa)	0.110	0.462
	Standard deviation of means (GPa)	0.186	0.683

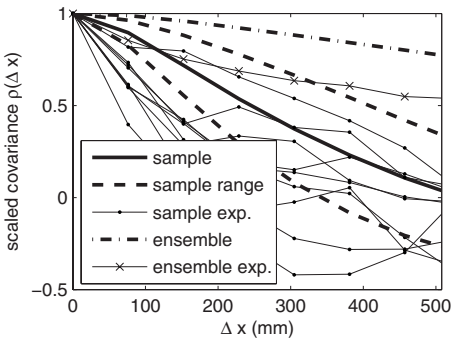

Fig. 9. Experimental and simulated scaled autocovariance functions for B samples estimated by ensemble and sample methods

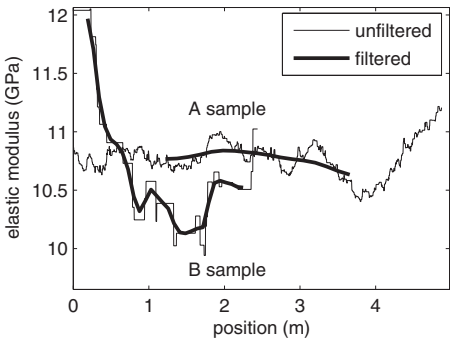

Fig. 10. Filtered and unfiltered sample modulus processes generated by simulation for A and B type samples showing increased smoothing for the A samples due to longer test span

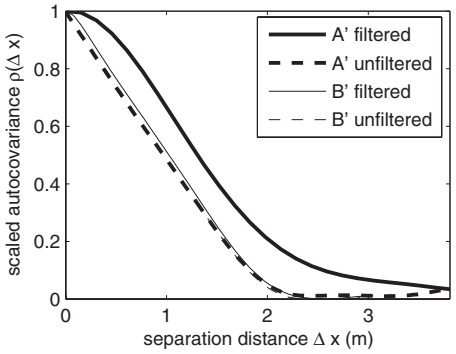

Fig. 11. Scaled autocovariance functions for filtered and unfiltered A' and B' type samples obtained by simulation of specimens longer than those tested experimentally showing independence of covariance with respect to the cross-sectional size and the increased effect of spatial averaging in the A samples

consistent with the difference between those functions for a process with and without an additive white noise term. It is beyond the scope of this paper to specifically address the magnitude of the noise, or additional uncertainty, present in measurements of the PSL bending elastic modulus, but at this point it suffices to observe that the point statistics and scaled autocovariances obtained from simulated PSL bending tests are consistent with those obtained experimentally.

Simulation Results

Having validated the computational model, simulation is now be used to characterize the elastic modulus process. The computational model allows the direct determination of the elastic modulus process underlying the elastic modulus process filtered by bending tests. First, simulations of A and B samples are used to show the statistical differences between the unfiltered modulus process $E(x)$ and the filtered process $\bar{E}(x)$. The filtered process is calculated from the simulated unfiltered process by performing virtual bending tests using Eqs. (10) and (3). The result is a weighted averaging of realizations $e(x)$ into realizations of the filtered process $\bar{e}(x)$, which is continuous, in contrast to the piecewise constant process $e(x)$.

Comparison of Filtered and Unfiltered Elastic Modulus Processes

Fig. 10 shows one each of a simulated A sample and simulated B sample of $E(x)$ along with its filtered counterpart $\bar{E}(x)$. The averaging that takes place during a bending test can be observed in the smoothed character of the samples of $\bar{E}(x)$. The samples of $E(X)$ are piecewise constant due to the assumption that elastic constants do not vary within the strands. Therefore, at each location in the PSL member where a strand ends, the cross-sectional modulus changes abruptly. The spacing between discontinuities in the sample of $E(x)$ for the A sample is much smaller than for the B sample. This is because there are many more strands in the A sample cross section, and so the frequency of strand endpoints is higher than in the B samples. Finally, The averaging effect is much stronger in the A sample due to the 2.44 m span of the bending tests on A samples. This span is much longer than the 0.381 m span used for the B samples, and therefore the averaging takes place over a much larger volume of material. The figure also reflects the different lengths of the A and B samples.

Fig. 11 shows ensemble scaled autocovariance functions for the filtered and unfiltered elastic modulus processes for samples with all geometric parameters as in Table 1 except that the lengths of the samples are increased to 6.35 m and 5.08 m respectively for samples with cross section corresponding to the A and B samples. The samples with longer length are denoted A' and B' samples. 250 A' and 250 B' samples are generated and analyzed to obtain better estimates of the second moment properties of the elastic modulus process.

The two main features of the results shown in Fig. 11 are that the A' samples show a significant difference between the filtered and unfiltered scaled autocovariance functions, and that the scaled autocovariance functions for the unfiltered A' and B' samples are nearly identical. The bending test span of the A' samples, 2.44 m, is long enough that significant averaging of the elastic modulus takes place. This averaging tends to smooth high frequency oscillations in the elastic modulus process, and results in higher covariance values at small separation distances. For a bending test span of 0.381 m, as used for the B' sample simulations, this averaging effect becomes negligible. The second feature, that the scaled autocovariance of the unfiltered A' and B' samples are nearly identical, arises because the decay of covariance is controlled by the frequency of strand ends. Though the A' samples have a larger cross section than the B' samples, meaning that the end of an individual strand will have less effect on the cross-sectional modulus of an A' sample, the presence of many more strands in the A' cross section means that strand ends occur more frequently than in the B' samples. The simulation data indicate that these effects counteract one another, rendering the scaled autocovariance of the unfiltered PSL elastic modulus process independent of the number of strands in the cross section.

These results also indicate that one must be careful in using bending tests to determine the spatial variation of elastic properties in PSL members, although the same would be true for dimensional lumber. The experimenter should select a span for the bending tests that is as short as possible to reduce the averaging effect, but is not so short as to result in appreciable shear deformation, which would contaminate the test results. For members with cross sections typical for light-frame construction the averaging effect appears to be minimal, but for members such as those used in post-and-beam construction, or as primary members in bridge trusses, the effect can be substantial. Even using a machine with continuous recording ability, as is done in machine stress

Table 5. Point Statistics of Filtered and Unfiltered Simulated Modulus Processes

Statistic	A' unfiltered	A' filtered	B' unfiltered	B' filtered
Mean (GPa)	10.8	10.8	10.9	10.9
Standard deviation (GPa)	0.248	0.220	0.827	0.806
Skewness	−0.11	−0.16	−0.1	−0.1
Kurtosis	2.94	2.97	2.99	2.97

rated lumber, would not mitigate this problem since a sufficient span must be used to render shear deformations negligible.

Table 5 shows that the one-point statistics of the filtered and unfiltered elastic modulus processes are nearly identical for both the A' and B' samples. Filtering through virtual bending tests results in small reductions in the standard deviation and kurtosis for both A' and B' samples. The effect is so small as to be difficult to distinguish from estimation error, but, to the extent it is a real feature of the data, it is likely caused by the tendency of the filtering to remove extreme values from the elastic modulus process. From this point forward, consideration is restricted to the unfiltered elastic modulus process as determined by simulation of the PSL mesostructure and application of the rule of mixtures [Eq. (9)] at each cross-section.

Probabilistic Model for PSL Elastic Modulus Process

The elastic modulus process $E(x)$ is assumed to be stationary in the weak sense and ergodic. This section presents a probabilistic model for the process based on these assumptions, and complete through second moment properties and marginal distribution.

The one-point statistics of Table 5 give a strong indication that the marginal distribution of $E(x)$ is Gaussian, which is expected since Eq. (9) contains a summation of independent, identically distributed random variables $E_x[C(\Theta_i)]$, allowing the invocation of the central limit theorem. For PSL, the marginal distribution of $E(x)$ becomes very nearly Gaussian when ten strands are included in the cross section.

The cross-sectional modulus is approximated in this study as the sum of a set of independent identically distributed random variables $E_x[C(\Theta_i)]$. The variance of $E(x)$ is therefore given by

$$\text{var}[E(x)] = \frac{\text{var}\{E_c[C(\Theta_i)]\}}{n_s} \tag{11}$$

Based on simulations of PSL members with 24, 75, 150, and 275 strands, the standard deviation σ_E of $E(x)$ in a PSL member with n_s strands in its cross section is given by

$$\sigma_E = \frac{4.07 \text{ GPa}}{\sqrt{n_s}} \tag{12}$$

Note that these experiments and computations do not demonstrate the presence or absence of a size effect on the mean elastic modulus of PSL. This is an important issue that is significant in the design of sawn-lumber structures, and should be investigated for PSL.

The unfiltered elastic modulus process $E(x)$ is modeled as a Gaussian random process with continuous samples. This model does not have the ability to reproduce the discontinuities in samples of $E(x)$ that occur whenever a strand ends. These discontinuities in the mesostructure may play in important role in the onset of damage processes in PSL, but are considered to be minimally important with respect to the elastic properties of PSL members. Calibration of the model is provided by the mean, 10.8 GPa, the standard deviation given by Eq. (12), and the scaled autocovariance function. Fig. 11 shows that the scaled autocovariance function of a PSL member is independent of the number of strands in the cross section. This is true as long as there are more than roughly ten strands in the cross-section.

A good functional fit to the scaled autocovariance function of the unfiltered elastic modulus process has linear decay from one to zero over a specified separation distance, and zero value for greater separation distances. The general form of such a function is

$$\rho(\Delta x) = \begin{cases} 1 - \dfrac{\Delta x}{l_{c0}}, & \Delta x \le l_{c0} \\ 0, & \Delta x > l_{c0} \end{cases} \tag{13}$$

with best fit parameters to the data of Fig. 11 of $l_{c0} = 1.95$ m. This function gives an excellent approximation to the estimated scaled autocovariance over the range of separation distances where the value of $\rho(\Delta x)$ is greater than 0.1. The choice of this scaled covariance function implies that the process $E(x)$ is not differentiable. This is realistic since the mesostructural model results in a process $E(x)$ that is piecewise constant, but is not consistent with the choice of a continuous Gaussian process as the probabilistic model. This inconsistency may cause problems in exact calculations, but should not affect simulations used in Monte Carlo approaches. If differentiability of the modulus process were required for calculations an alternative form could be fit to the scaled autocovariance. The corresponding spectral density function is

$$s(\omega) = \frac{l_{c0} \sin^2(\omega l_{c0}/2)}{\pi(\omega l_{c0}/2)^2} \tag{14}$$

which is useful in generating realizations of the modulus process using the spectral representation (Soong and Grigoriu 1992)

Conclusion

Three point bending tests on PSL members of different cross-sectional size show that the variability of the elastic modulus in PSL is substantially lower than that for equivalent-sized solid lumber, and that the elastic modulus varies as a stochastic process with correlation length of several tens of inches. Estimation of the spatial variation of the elastic modulus requires physical testing of an ensemble of specimens because commonly available specimens are not long enough to allow the assumption of ergodicity.

A computational model for the cross-sectional stiffness of PSL members includes uncertainty in the strand length, strand elastic constants, and grain angle, and is validated against the experimental measurements, indicating that it can be used as a predictive tool for PSL elastic modulus. The computational model is used to further investigate the features of the elastic modulus process. Model results show that when the PSL member contains more than about 100 strands, the span used in bending tests is long enough that the measured modulus process is distorted by the averaging that takes place over the material volume of the test. PSL elastic modulus is found to be Gaussian, with variance that scales inversely with the square of the number of strands in the cross section, and the modulus process is found to have a scaled covariance structure that is independent of the number of constituent strands. A mathematical model for the elastic

modulus process is introduced that can be used in reliability analysis of PSL members in which stiffness uncertainty is to be considered.

Acknowledgments

M. Peterson at the Wood Mechanics Laboratory provided valuable assistance in preparing test specimens and conducting the laboratory experiments. The National Science Foundation partially supported this work through Grant No. CMMI-0826265.

Notation

The following symbols are used in this paper:

A = specimen Group A;
A' = simulated specimens;
B = specimen Group B;
B' = simulated specimens;
C = elastic constitutive matrix;
d = midspan displacement during bending test;
d_s = wood strand depth;
$\bar{E}_i$ = filtered elastic modulus process at position x_i;
$E_{x'}$ = orthotropic elastic constant;
$E_{y'}$ = orthotropic elastic constant;
$E(x)$ = elastic modulus process;
$\bar{E}(x)$ = filtered elastic modulus process;
$\bar{e}(x)$ = realization of $\bar{E}(x)$
$e(x)$ = realization of $E(x)$;
$\bar{e}_i$ = realization of $\bar{E}_i$;
e_i = realization of E_i;
$f_\theta(\theta)$ = probability density function of grain angle;
$f_{\theta,\mathrm{sym}}(\theta)$ = one-sided probability density function of grain angle;
$G_{x'y'}$ = orthotropic elastic constant;
I = moment of inertia;
L_s = strand length;
l_m = length of test specimen;
l_p = spacing of bending tests;
l_t = bending test span;
l_c = correlation length;
l_{c0} = scaled autocovariance parameter;
m = bending moment;
m_o = number of observations along the length of a sample stochastic process;
n_t = number of bending tests along specimen length;
n_s = number of strands in PSL cross section;
p_i = load applied at test point i during bending test;
$s(\omega)$ = spectral density function;
w = test specimen cross-sectional width;
w_s = wood strand width;
x = position along length of PSL member;
x_i = position of bending test;
x' = strand coordinate axis;
y_{ij} = realization i of $Y(x)$ at x_i;
$Y(x)$ = an arbitrary stochastic process;
Z = a β random variable;
α = parameter of the β distribution;
β = parameter of the β distribution;
Δx = separation distance;
Θ = wood grain angle;
$\nu_{x'y'}$ = orthotropic elastic constant;
$\rho(\Delta x)$ = scaled autocovariance;
σ_E = standard deviation of $E(x)$; and
σ_Y = standard deviation of $Y(x)$.

References

ASTM. (2005). "Standard methods of static tests of lumber in structural sizes." *D198-05*, West Conshohoken, Pa.

Bejo, L., and Lang, E. (2004). "Simulation based modeling of the elastic properties of structural composite lumber." *Wood Fiber Sci.*, 36, 395–410.

Clouston, P. (2006). "Characterization and strength modeling of parallel strand lumber." *Holzforschung*, 61, 392–399.

Clouston, P., and Lam, F. (2001). "Computational modeling of strand-based wood composites." *J. Eng. Mech.*, 127, 844–851.

Clouston, P., and Lam, F. (2002). "A stochastic plasticity approach to strength modeling of strand-based wood composites." *Compos. Sci. Technol.*, 62, 1381–1395.

Ekevad, M. (2004). "Method to compute fiber directions in wood from computed tomography images." *Wood Sci.*, 50, 41–46.

Forest Products Laboratory. (1999). *Wood handbook: Wood as an engineering material*, U.S. Department of Agriculture, Madison, Wis.

Jones, R. M. (1975). *Mechanics of composite materials*, McGraw-Hill, New York.

Lam, F., and Varoglu, E. (1991a). "Variation of tensile strength along the length of lumber. Part 1: Experimental." *Wood Sci. Technol.*, 25, 351–359.

Lam, F., and Varoglu, E. (1991b). "Variation of tensile strength along the length of lumber. Part 2: Model development and verification." *Wood Sci. Technol.*, 25, 449–458.

Lam, F., Wang, Y.-T., and Barrett, J. D. (1994). "Simulation of correlated non-stationary lumber properties." *J. Mater. Civ. Eng.*, 6, 34–53.

Soong, T. T., and Grigoriu, M. (1992). *Random vibration of mechanical and structural systems*, Prentice-Hall, Upper Saddle River, N.J.